

Journal of Materials Chemistry A

Accepted Manuscript



This is an *Accepted Manuscript*, which has been through the Royal Society of Chemistry peer review process and has been accepted for publication.

Accepted Manuscripts are published online shortly after acceptance, before technical editing, formatting and proof reading. Using this free service, authors can make their results available to the community, in citable form, before we publish the edited article. We will replace this *Accepted Manuscript* with the edited and formatted *Advance Article* as soon as it is available.

You can find more information about *Accepted Manuscripts* in the [Information for Authors](#).

Please note that technical editing may introduce minor changes to the text and/or graphics, which may alter content. The journal's standard [Terms & Conditions](#) and the [Ethical guidelines](#) still apply. In no event shall the Royal Society of Chemistry be held responsible for any errors or omissions in this *Accepted Manuscript* or any consequences arising from the use of any information it contains.

**Simultaneous Visual Detection and Removal of Lead(II) Ions with Pyromellitic
Dianhydride-Grafted Cellulose Nanofibrous Membranes**

Yan Li,^a Yanan Wen,^a Lihuan Wang,^a Jianxin He^b, Salem S. Al-Deyab,^c Mohamed

El-Newehy,^{c, d} Jianyong Yu^e and Bin Ding,^{a, b}*

^a Key Laboratory of Textile Science & Technology, Ministry of Education, College of Textiles, Donghua University, Shanghai 201620, China

^b College of Textiles, Zhongyuan University of Technology, Zhengzhou 450007, China

^c Petrochemical Research Chair, Department of Chemistry, College of Science, King Saud University, Riyadh 11451, Saudi Arabia

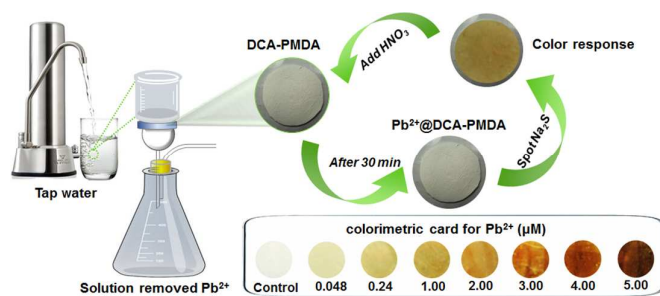
^d Department of Chemistry, Faculty of Science, Tanta University, Tanta 31527, Egypt

^e Nanomaterials Research Center, Modern Textile Institute, Donghua University, Shanghai 200051, China

** Corresponding author at: Key Laboratory of Textile Science & Technology, Ministry of Education, College of Textiles, Donghua University, Shanghai 201620, China.*

Fax: +86 21 62378392.

E-mail: binding@dhu.edu.cn (B. Ding)



Simultaneous Colorimetric Assay and Removal of Lead(II) Ions with Pyromellitic Dianhydride-Grafted Cellulose Nanofibrous Membranes

Simultaneous Visual Detection and Removal of Lead(II) Ions with Pyromellitic Dianhydride-Grafted Cellulose Nanofibrous Membranes

Cite this: DOI: 10.1039/x0xx00000x

Yan Li,^a Yanan Wen,^a Lihuan Wang,^a Jianxin He^b, Salem S. Al-Deyab,^c Mohamed El-Newehy,^{c, d} Jianyong Yu^e and Bin Ding,^{a, b*}

Received 00th January 2012,
Accepted 00th January 2012

DOI: 10.1039/x0xx00000x

www.rsc.org/

By virtue of the affinity of pyromellitic dianhydride (PMDA) with Lead(II) ion (Pb^{2+}) and inherent structure merits of electrospun nanofibrous membrane, a novel solid-phase nanofibrous material was facilely fabricated by modification deacetylated cellulose acetate membrane with PMDA (DCA-PMDA). The resultant DCA-PMDA can be applied for naked eye detection and removal of Pb^{2+} from water matrixes simultaneously by a simple filtration and follow with Na_2S solution treatment. Importantly, the color of the DCA-PMDA exclusively changes from white to dark yellow-brown owing to form the deposit of PbS , which can be applied for colorimetric detection of Pb^{2+} with a naked eye detection limit of $0.048 \mu\text{M}$. Under the same circumstance, the maximum adsorption capacity was determined to be as high as 326.80 mg/g . Furthermore, the extraction of Pb^{2+} from the DCA-PMDA was possible with HNO_3 . The regenerated membrane that remained maintained the high sensitivity to Pb^{2+} and exhibited almost the same adsorption capacity as that of the original one. Therefore, the proposed membrane offered a cost-effective material and may be considered a viable alternative for effectively detecting and enriching toxic Pb^{2+} from water samples.

Introduction

Multivalent transition metals exist in natural and contaminated environments and cannot be easily detoxified *via* degradation, resulting in their persistence in the environment¹⁻³. Lead(II) ion (Pb^{2+}), as a member of multivalent transition metals, is a longstanding environmental contaminant since it can be taken into the body through the pulmonary system via the digestive system through contaminated water or food⁴. An excess of Pb^{2+} in the human body affects the heart, bones, kidneys, and nervous system⁵. The presence of Pb^{2+} is especially dangerous for children because it interferes with the development of the nervous system and results in permanent learning and behavior disorders⁶⁻⁸. Meanwhile, Pb^{2+} can be easily encounter in the environment due to its previous or present applications in batteries, gasoline, pigments, etc. The increasing threatens of toxic Pb^{2+} to human beings triggered the World Health Organization (WHO) and European Commission strictly set the maximum permissible contamination level in drinking water as $0.048 \mu\text{M}$ in 1996⁹.

Concerns over toxic exposure to Pb^{2+} have motivated the exploration of new Pb^{2+} detecting or removing methods, so as to meet the WHO's standard¹⁰. To date, the majority of Pb^{2+}

detection and removal tasks have been performed separately. For instance, various colorimetric sensors can efficiently detect Pb^{2+} , colorimetric assay is an attractive technology for fabricating simple, low-cost, and portable analytical devices^{11, 12}. Jiang *et al.* developed a colorimetric method for Pb^{2+} using papain-functionalized gold nanoparticles, naked eye detection limit is $2 \mu\text{M}$ ¹³. Molina *et al.* found that 2-Ferrocenylimidazo pyridine could be applied for colorimetric detection based on its deazapurine ring, and its corresponding naked eye detection limit is $100 \mu\text{M}$ ¹⁴. It is obviously that the existing colorimetric sensors are insufficient to meet the demand of WHO since average concentration of metals in nature water is so low. And immobilization of these sensors at a high concentration has not been demonstrated in most cases, making it difficult to effectively remove Pb^{2+} at the same time.

In parallel with development of detecting methods, many techniques (such as adsorption, flocculation-coagulation, photocatalysis, biological degradation, and chemical oxidation) have been utilized to remove Pb^{2+} ¹⁵⁻¹⁸. The adsorption method is a cost effective one, which also offers great flexibility in design and operations. However, the application of adsorbents often requires post treatment after adsorption. Meanwhile, only a few adsorbents based on mesoporous silica monoliths are

capable to removal and detect Pb^{2+} contaminant simultaneously. Unfortunately, those adsorbents suffer from complex fabrication process and low adsorption capacity due to its straight and narrow pore channels, in which molecular diffusion and transportation is limited¹⁹⁻²¹. Therefore, there is a growing need for a sensor with high sensitivity, selectivity and adsorption capacity is essential to maintaining the maximum permissible limit and protecting public health.

Since its discovery in 1745, electrospun nanofiber has been considered as an extremely versatile sensing platform and adsorbent owing to its unique three-dimensional (3D) fibrous structure with high open porosity and interconnected porous structure²²⁻²⁴. Previous researches have suggested that nanofiber as a sensing platform would endow the sensors enhanced portability, stability and improved sensitivity²⁵⁻²⁸. When it act as adsorbent, interconnected 3D porous structure of nanofibrous membrane (NFM) may promote molecular diffusion and transportation²⁹. Furthermore, it is known that the adsorption process can be limited by diffusion into the closed pores of common adsorbents, while in the NFM, their open pores and 3D interconnected pore channels could overcome the problem^{30, 31}. Especially its self-standing non-woven fabric like structure, ease of incorporation of specific functionality, and extraordinary physical and chemical properties, offer improved efficiency and omit the additional post treatment after adsorption in the field of water contaminator removal. By all accounts, NFM could be one of the suitable candidates to detect and enrich Pb^{2+} simultaneously.

Herein, an intriguing and economic pyromellitic dianhydride (PMDA) grafted deacetylated cellulose acetate (DCA-PMDA) NFM with dual functions: adsorption (through filtrating process) and colorimetric detection (through Na_2S color produce reaction) of Pb^{2+} in the polluted water has been identified and prepared. As an environmentally friendly molecule, PMDA perform very well as a grafting agent for adsorbents because it can readily react with hydroxyl or amide groups and at a same time introduce large amounts of carboxyl groups on the adsorbents, which can improve the adsorption capacity for Pb^{2+} ^{32, 33}. The resultant NFM is expected to possess high selectivity to Pb^{2+} due the mask effect of iminodiacetic acid (IDA), excellent sensitivity and high adsorption capacity is achieved by optimizing several parameters such as PMDA graft amount, solution pH and contact time. In addition, the NFM would be cost effective based on the reversibility and reusability performances over many cycles without lost its functionality.

Experiments

Materials and reagents.

CA with the acetyl content of 39.8 wt% ($M_w = 30\ 000$) was purchased from Sigma Aldrich. Inc. USA. PMDA, *N,N*-dimethylacetamide (DMAc), sodium sulphide (Na_2S), NaOH, HNO_3 , above five reagents were provided by Aladdin Co., Ltd.,

China. *N,N*-dimethylformamide (DMF), IDA and acetone were provided by Shanghai Chemical Reagents Co., Ltd. The standard Pb^{2+} and other metal ions solutions (K^+ , Ca^{2+} , Cu^{2+} , Mn^{2+} , Ni^{2+} , Cd^{2+} , Fe^{3+} , and Zn^{2+}) for evaluating the selectivity were prepared from their corresponding AAS grade ($1000\ \mu\text{g mL}^{-1}$) solutions and purchased from Wako Pure Chemicals, Osaka, Japan. The solution pH was measured by using a PHS-3C pH meter (Shanghai Precision Scientific Instrument Co., Ltd., China). Filter paper was supplied by Hangzhou Special Paper Co., Ltd., China. Ultra-pure water with a resistance of $18.2\ \text{M}\Omega$ was prepared by a Heal-Force system. All chemicals were of analytical grade and used as received.

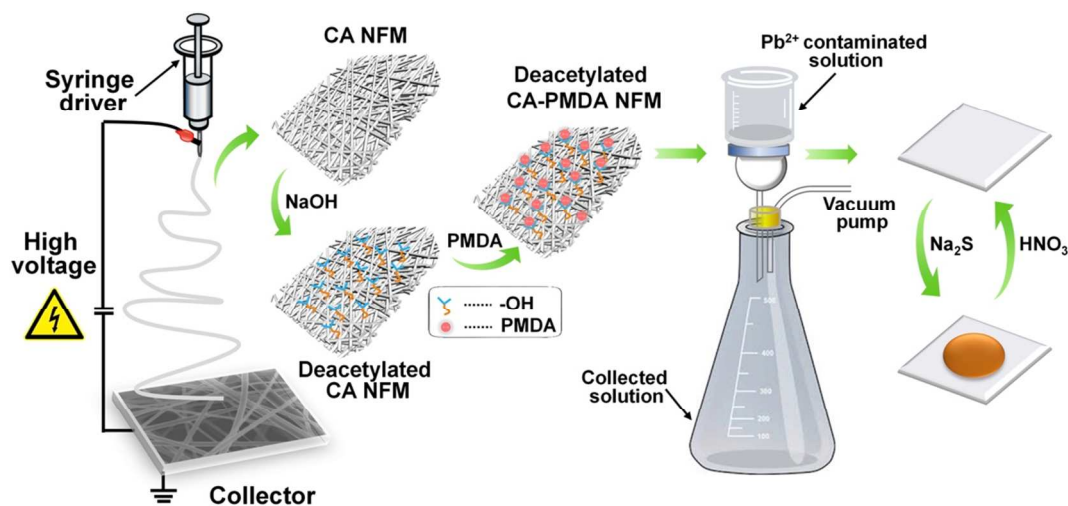
Fabrication and Deacetylation the CA NFM *via* Electrospinning.

Briefly, the 15 wt% CA precursor solution was prepared by dissolving 6 g of CA in 32 g of DMAc-acetone mixture (weight ratio of 1 : 2) with stirring for 12 h. Then, above solutions were fed through a capillary tip using a syringe (10 mL), the anode of the high voltage power supply was clamped to syringe needle tip and the cathode was connected to a collector (distance from the tip to the collector: 15 cm). During the electrospinning, the applied voltage was 20 kV, and the flow rate of the composite polymer solution was $0.5\ \text{mL h}^{-1}$ by using DXES-1 spinning equipment (Shanghai Oriental Flying Nanotechnology Co., Ltd., China). The electrospinning chamber was kept under a constant temperature range ($23 \pm 2\ ^\circ\text{C}$) and relative humidity ($55 \pm 3\ \%$). Following this, The CA NFM was heated in an oven at $200\ ^\circ\text{C}$ for 1 h and peeled off the slick paper carefully. The morphology of NFM was examined by using a field emission scanning electron microscopy (FE-SEM, S-4800, Hitachi Ltd., Japan). Apart from that, the Brunauer-Emmett-Teller (BET) surface areas of membranes were characterized by using N_2 adsorption-desorption isotherms with a surface area analyzer (ASAP 2020, Micromeritics Co., USA).

Deacetylation process of CA NFM was based on a previously reported method³⁴. By soaking the CA NFM (4 g) in 0.05 M NaOH (400 mL) for 4 days followed by washing with ultra-pure water to obtain neutral pH. Then it was dried and stored in a desiccator before use.

Preparation of PMDA-grafted deacetylated CA NFM.

A modification procedure for fabricating DCA-PMDA NFM was demonstrated here. Before functionalization, the DCA NFM was shaken twice with ethanol and followed with toluene to remove water. In subsequent procedure, a 250 mL round bottomed flask was applied, then DCA NFM and PMDA were added together to 30 mL of DMF, the weight ratios of DCA with PMDA in the DMF are 1/1, 1/2, 1/3 and 1/4 respectively. The preparation of filter paper-PMDA was same as above, and the weight ratio of filter paper with PMDA is 1/3. Those corresponding treated DCA NFM are named as $\text{DCA}_x\text{-PMDA}_y$ ($x/y = m_{\text{DCA}}/m_{\text{PMDA}}$). After stirring at $50\ ^\circ\text{C}$ for 5 h, the DCA-PMDA NFM was obtained, and it was washed in order with 0.1 M of NaOH and ultra-pure water. Then it was dried and stored



Scheme 1. Schematic illustration of the fabrication procedure of the DCA-PMDA NFM and simultaneous colorimetric detection and enrichment of target Pb^{2+} by DCA-PMDA NFM.

in a desiccator at room temperature before use. The surface chemical structures of CA, DCA as well as DCA-PMDA NFM were characterized using a Nicolet 8700 Fourier transform infrared (FT-IR) spectrometer in the $4000\text{--}400\text{ cm}^{-1}$ range in four replicate scans. The pore size of above mentioned membranes were tested by utilizing a capillary flow porometer (CFP-1100AI, Porous Materials Inc., USA).

Pb^{2+} enrichment, colorimetric detection and reuses studies

The DCA-PMDA NFM was sandwiched in a home-made poly(methyl methacrylate) flow cell, as shown in Fig. S1. A predetermined amount of solutions (50 mL) containing different concentrations of Pb^{2+} and 1 mM IDA were placed at top of the setup. With the application of vacuum pressure, the solutions were drawn to pass through the membrane. The flow rates through the membrane could be adjusted by the throttle value. After the Pb^{2+} being uptake by the DCA-PMDA NFM, the dosage and surface area of DCA-NFM is 2.77 mg and 1.74 cm^2 , respectively. The solutions after treated with NFM were collected by the bottom flask for measuring the residual Pb^{2+} concentrations. All the filtration processes were carried out at room temperature. And Pb^{2+} concentrations in before and after filtration were analysed by a Leeman Prodigy inductively coupled plasma atomic emission spectroscopy (ICP-AES). The resulting flux of DCA-PMDA is calculated based on the following equation: $\text{Flux} = Q_p/A_m$, where Q_p is filtrate flow rate through membrane (L/h), A_m is surface area of membrane (m^2). The amount of Pb^{2+} adsorbed on the DCA-PMDA NFM was calculated according to the following equation (1): $q_e = (C_0 - C_e) \times V/m$, where C_0 and C_e are the initial and equilibrium Pb^{2+} concentrations (mg L^{-1}), respectively. V is the volume of the solution (L) and the m is the weight of the membrane used (mg). The rejection coefficient (R) of DCA-PMDA NFM is calculated by: $R = 1 - (C_e/C_0)$. After the enrichment being finished, the DCA-PMDA NFM was took out and washed with

ultra-pure water for several times. The existence of Pb^{2+} on the NFM was confirmed by energy-dispersive X-ray (EDX) spectrometer (Hitachi S-4800, Hitachi Ltd., Japan).

The colorimetric detection procedure was carried out by treating the Pb^{2+} enriched NFM with 3% aqueous Na_2S solution at first. Then a dark brown spot appeared on the DCA-PMDA NFM owing to generation of PbS as shown in Scheme 1. Pb^{2+} retained on the NFM were analyzed by IS-30-6-R integrating sphere (Ideaoptics Technology Ltd., China) attached to the Ideaoptics PG 2000+ fiber optic spectrometer. A similar procedure was also carried out for different metal ions (Ca^{2+} , Zn^{2+} , Cu^{2+} , etc.)

In order to evaluate the reusability of the DCA-PMDA NFM, elution experiment was conducted with monoprotic acid. First, 50 mL of $5\text{ }\mu\text{M}$ Pb^{2+} solution was filtrated by DCA-PMDA NFM and treated with 0.4g 3% Na_2S , then the elution experiment was carried out using 3 M HNO_3 . After the membrane with dark yellow-brown color soaked in HNO_3 solution for 1 min, the washing step carried out with ultra-pure water for several times and then dried the membrane in the air. Subsequently, the DCA-PMDA NFM was reused in several cycles and clarifies long-term use as cost-effective material. The structure and property of DCA-PMDA after 10 times of HNO_3 treatment were investigate by FE-SEM and FI-IR. All experiments in this study were duplicated to assure the consistency and reproducibility of the results.

Result and Discussion

The effects of PMDA on the morphologies and functionality.

The morphological changes brought about by the deacetylation procedure with NaOH and modification process with PMDA were studied using SEM. The representative FE-SEM image of CA nanofibers revealed as 3D nonwoven membranes like structure, which consisted of randomly oriented nanofibers with

an average diameter of 267 nm in Fig. S2a. A few of groove structure on the CA fiber surface could be noted from the high magnification FE-SEM image. After treated with NaOH solution, the 3D membrane structure and surface morphology of DCA (Fig. S2b) remain essentially unchanged comparing with CA, while the average diameter of DCA increased to 282 nm.

The effect of PMDA amount on membranes morphology was investigated by introducing different amount of PMDA (the weight ratios of DCA with PMDA in the DMF are 1/1, 1/2, 1/3 and 1/4 respectively). The representative FE-SEM images presented in Fig. 1 indicated that all the samples possess two kinds of morphological features: 1) wrinkled fiber surface, and 2) obviously adhesions (indicated by dotted circle) among adjacent fibers after modification. The average diameters of relevant DCA₁-PMDA₁, DCA₁-PMDA₂, DCA₁-PMDA₃ and DCA₁-PMDA₄ were 290, 306, 315, and 320 nm, respectively. Due to the chemical etching effect of PMDA and processing solution impregnated in fibers during the modification, the average diameter, surface roughness and the adhesion structure among fibers increase gradually with the increasing of PMDA amount. It is worthy to note that due to the limited solubility of the PMDA in DMF, some particle agglomeration structures could be found on the nanofibers surface of DCA₁-PMDA₄ as well as among the voids.

To further explore the effect of PMDA amount on colorimetric detection performances and enrichment feasibility of DCA_x-PMDA_y to Pb²⁺, we carried out the analyses by cutting the DCA_x-PMDA_y into square and sandwiched in a flow cell. Then a 50 mL, 5 μM Pb²⁺ solution was continuously filtered through the membrane at a constant rate (2 mL/min). After 25 min, the Pb²⁺ adsorbed on the DCA_x-PMDA_y was signaled by spotting them with 0.04 g of 3 % Na₂S, and the Pb²⁺ are changed into colored PbS deposits. It is easy to find that when the weight ratios of DCA with PMDA increases from 1/1 to 1/3, the colorimetric responses increase, hinting that PMDA amount is a crucial influence factor for Pb²⁺ adsorption and detection. However, as PMDA amount increases, the insoluble PMDA directly leads the unevenly distribution of functional group, so as the DCA₁-PMDA₄ shows an uneven color (insets in Fig. 1d). In this case, we recruited DCA₁-PMDA₃ as a platform for subsequent exploration. The enrichment of Pb²⁺ on the fiber surface was also conformed by EDX, as shown in Fig. S3, the Pb element with the content of 1.78% was identified in the DCA₁-PMDA₃. The affinity between DCA₁-PMDA₃ and Pb²⁺ is ascribed to the —COOH groups distribute on the DCA-PMDA, those functional groups could easily interact with Pb²⁺ by forming the Pb²⁺-carboxyl coordination (insets Fig. S3) in which the Pb²⁺ is bound by both carboxyl oxygen atoms (C=O...Pb²⁺)³⁵⁻³⁶.

The surface chemical structures of CA, DCA and DCA₁-PMDA₃ NFM were studied by ATR-FTIR spectroscopy, as shown in Fig. S4. Compared with CA NFM, the FTIR spectrum of DCA NFM showed a new peak at 3452 cm⁻¹, which is corresponded to the stretching vibration of hydroxyl group, and

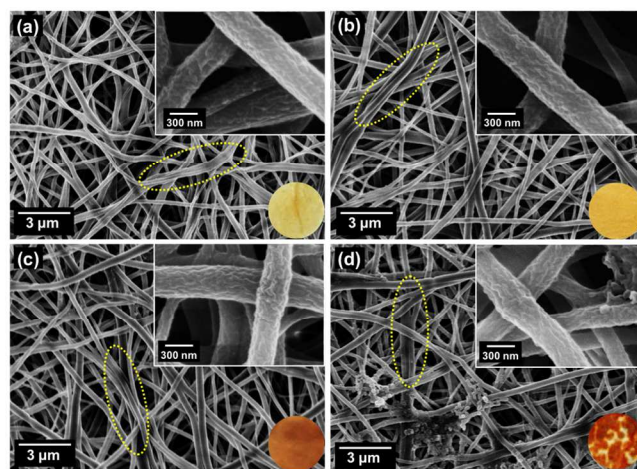


Fig. 1. FE-SEM images of (a) DCA₁-PMDA₁, (b) DCA₁-PMDA₂, (c) DCA₁-PMDA₃, and (d) DCA₁-PMDA₄. Insets are the corresponding images at high magnification and optical images of each sample after incubation with 5 μM Pb²⁺ followed with Na₂S treatment.

the absorption peak of 1744 cm⁻¹ which is assigned to the stretching vibration of C=O of ester disappears. Above changes all demonstrate the progressive hydrolysis of the acetyl groups^{37, 38}, this is also consistent with the reaction displayed in Fig. S5. As shown in the FTIR spectrum of DCA-PMDA NFM, a new peak at 1723 cm⁻¹, assignable to the C=O stretching of COOH is observed³⁹, provides preliminary evidence that the PMDA is anchored on the surface of DCA NFM.

Quantitatively analysis effect of modification process on porous structure.

Despite the PMDA already grafted on the surface of DCA NFM, it should be note that porous structure feature of NFM is another vital element which would greatly affect the Pb²⁺ adsorption property. Therefore, we next focused our attention on figuring out that whether the modification process had caused porous structural transformation or not. Here, the pore structure was measured through N₂ adsorption at 77 K. As shown in Fig. 2a, all curves exhibited the isotherm of type IV according to the IUPAC classification^{40, 41}. A series of typical adsorption behaviours including monolayer adsorption, multilayer adsorption and capillary condensation could be observed, revealing characteristics of mesopores within the as prepared membranes. And the narrow H1 hysteresis loop during the high-pressure region indicated that the mesopores are open, thus, there is no significant interruption between the capillary evaporation and condensation for N₂. The Brunauer-Emmett-Teller (BET) surface areas of CA, DCA and DCA₁-PMDA₃ NFM were inset in Fig. 2a, the BET surface area of DCA₁-PMDA₃ NFM shows a slightly decrease after two steps treatment due to the two kind of morphology changes: fiber diameter and surface roughness increase. And the changing trend of fiber diameter plays an even greater role in decreasing BET surface area^{42, 43}.

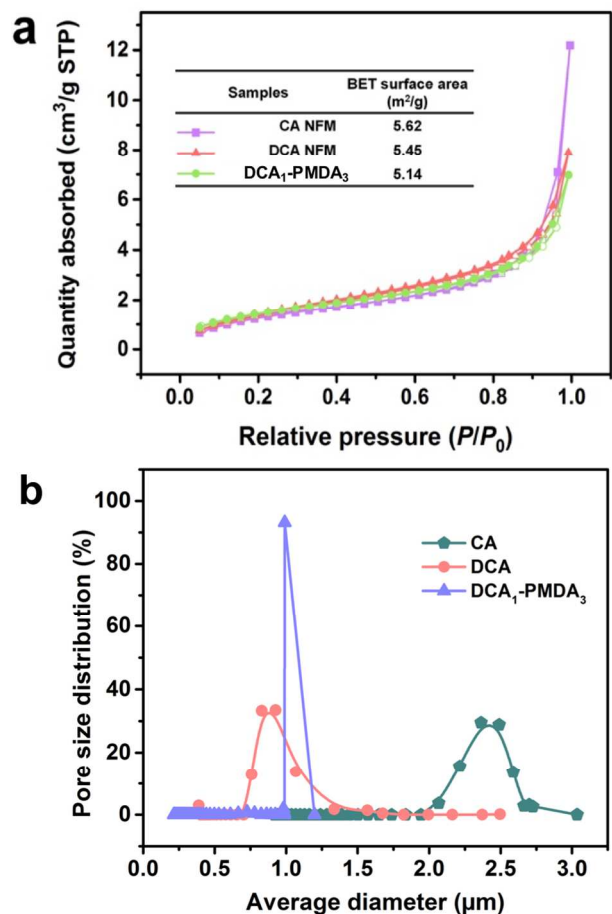


Fig. 2. (a) N₂ adsorption-desorption isotherms of relevant CA, DCA, and DCA₁-PMDA₃ samples. (b) Average pore size distribution curves of relevant samples.

The pore size of the relevant CA NFM (Figure 2b) revealed that the pore size distribution in the range of 0.2–3 μm with a well-developed peak centered at 2.36 μm. After deacetylation, the average pore size decreased to 0.99 μm ascribed to the growth of the nanofibers diameter and increase of packing density. Moreover, the NaOH solution surface tension would induce shrinking of NFM during the drying process, which reduces the pore size too. For DCA₁-PMDA₃, the average pore size is 0.721 μm and the uniformity of porous structure increase after modification due to the PMDA etching effect and the surface tension of DMF induced shrinkage. The tortuous porous structure in DCA₁-PMDA₃ could provide numerous interconnected microporous channels that significantly boom the active sites for ligands and Pb²⁺ adsorption. The aforementioned results also revealed that the structure of the fibrous membranes was maintained without dramatically change, and the large surface area and the porous structure could provide large quantity of active sites available for ligands and Pb²⁺ to binding. Therefore, the resultant nanofibrous membranes may be suitable for applications in practical Pb²⁺ purification.

Application for colorimetric detection of Pb²⁺.

Optimization of experimental conditions. The solution

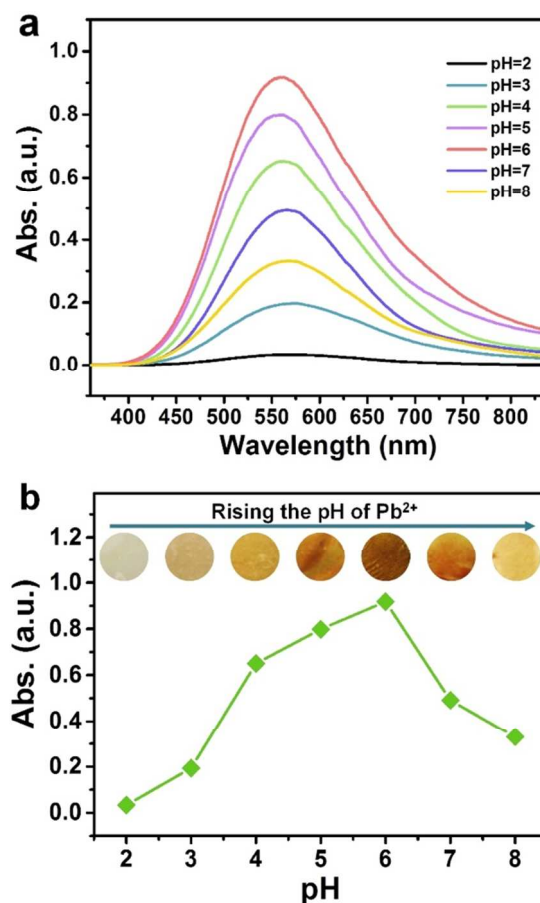


Fig. 3. (a) Effect of pH on the color response after filtrated 5 μM Pb²⁺ solution (50 ml) in 20 min. (b) The absorbance of respective strips at 560 nm versus different pH.

acidity plays an important role in detection of metal ions, since the solubility of metal ions, counter ions concentration to make the complexation with sensor platform's functional groups and also the ionization possibility of the platform during operation processes would be affected. So to comprehend the effect of solution pH on Pb²⁺ detection, the DCA₁-PMDA₃ based strip were treated by the above-mentioned Pb²⁺ adsorption and colored precipitation developing processes, and then those strips were studied at different pHs in the ranges of 2.0–8.0 subsequently. The UV-vis absorption spectra of each sample is depicted in Fig. 3a, it is obvious that except the sample exposure to the Pb²⁺ with an initial pH value of 2, all the rest samples show an absorption peak at 560 nm, hinting the effective formation of PbS on strip. The reason may be that in the acidic pH region, the sorption efficiency was low due to the availability of hydronium (H₃O⁺) ions on the strip surface, resulting in a poor sensing performance when the pH value of solution is 2. In a pH range from 3.0 to 6.0, the absorption intensity of samples was increased gradually with the increase of the pH and reaches the maximum when pH is ca. 6.0 (Fig. 4b). That is due to the less competitive interaction between the H₃O⁺ ions and Pb²⁺ for the same sorption sites on the strip surface⁴⁴. However, this increasing tendency has stopped by the water-insoluble lead hydroxide/oxide precipitated when the

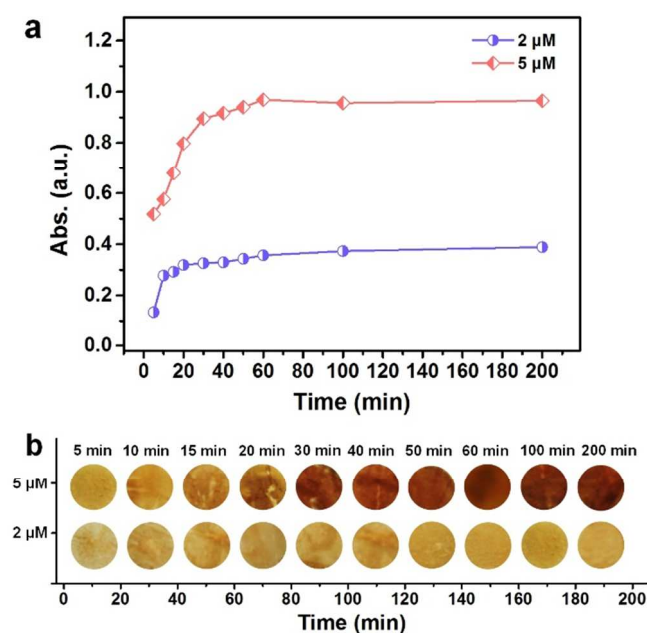


Fig. 4. (a) The plots of the absorption at 560 nm as a function of contact time, and (b) the corresponding optical images of the strip after filtrated 50 mL of 2 μM and 5 μM Pb^{2+} liquor.

pH value of solution is above 6 might be in the pH range from 7.0 to 8.0. On the other hand, the $-\text{COOH}$ group of PMDA has a pK_a value between 2 and 4. When pH values lower than the pK_a , $-\text{COOH}$ groups are predominantly positive charged, which would restrict access to adsorption sites by Pb^{2+} as a result of repulsive forces⁴⁵. When pH values higher than the pK_a , more $-\text{COOH}$ groups are negative charged, promoting the uptake of Pb^{2+} on the $\text{DCA}_1\text{-PMDA}_3$. Therefore, we select a pH value of 6.0 for all subsequent tests.

An adequate contact time is another important factor to affect the colorimetric response of the strip. Therefore, the effects of contact time on the sensing performance at different initial Pb^{2+} solution concentration (2 and 5 μM) were experimentally evaluated. The influence of contact time is obtained by continuously monitoring the UV-vis absorbance spectra of strips at a series of selected time points (5, 10, 15, 20, 30, 40, 50, 60, 100, and 200 min). Fig. 4a shows that a high uptake rate witnessed for the first 20 min, which could be explained by the availability of plenty adsorption sites on the strip at this time stage. As the Pb^{2+} getting attach to these sites with contact time, the amount of adsorbed Pb^{2+} gradually reaches a maximum when there is no more significant Pb^{2+} removal taking place. The adsorption equilibrium times of strip for Pb^{2+} are 5 and 30 min for the 2 and 5 μM initial Pb^{2+} solution, respectively. Similar adsorption behavior is reported in other literatures^{46,47}. The corresponding optical images shown in Fig. 4b show a good agreement with the kinetics of the strip. It can be seen that 5 μM Pb^{2+} -incubated strips showed distinguishable color changes at an initial time stage ($t < 30$ min). However, when further prolonging the reaction time, no significant color differences could be observed between the samples even the contact time was prolonged to 200 min. While, as for the 2 μM

Pb^{2+} -incubated strips, it is around 10 min that no further color change would happen among samples. Since we are aiming to develop strip for naked eye detecting and removing of trace Pb^{2+} , 30 min is chose as the optimum contact time to realize the maximum Pb^{2+} lowest naked eye detection limit and removal efficiency, and the corresponding flux of $\text{DCA}_1\text{-PMDA}_3$ is control as $574.7 \text{ L m}^{-2} \text{ h}^{-1}$ under this condition.

Colorimetric determination of Pb^{2+} . Fig. 5 shows the color change of strips at different concentration of Pb^{2+} between 0—5 μM . From Fig. 5a, it is easy to find that the absorbance intensity of strip at 560 nm increased gradually, suggesting an increase of PbS on the surface. A linear relationship between the absorption intensity and Pb^{2+} concentration over the range of 0.24 to 5 μM is also illustrated by the curve inset Fig. 5a. The optical images of strips toward various concentrations of Pb^{2+} , which were obtained under the optimal conditions, are presented in Fig. 5b. It could be seen that the strips displayed distinguishable color changes from white to dark yellow-brown color upon the increase of Pb^{2+} concentration, which could be clearly identified with naked eyes or a charge-coupled device camera. Moreover, it is worth pointing out that even the remarkably low concentration of Pb^{2+} ions could be detected by naked eye color test. In order to illustrate the excellent sensing performance, the naked eye detect limit of DCA-PMDA has been compared with other reported NFM based colorimetric sensors. From Table S1, we could find that the limitation of our strip can be achieved to 0.048 μM without the help of equipment, which is much lower than previously reported cases. In another words, the strip is good enough for detecting Pb^{2+} in drinking water without sample pretreatment according to the limit of 0.048 μM defined by the WHO. Furthermore, the detection limit of this strip could be much lower when prolongs the enrichment time or couples it with equipment.

To demonstrate the potential practical applications of our assay, the proposed DCA-PMDA NFM for determination and removal of Pb^{2+} levels was evaluated with two real water samples, one from the Jingyue Lake at our campus and another from domestic tap water. The water samples from lake have been filtered through a 0.2 μm membrane first, and the tap water is used without further treatment. Owing to the concentration of Pb^{2+} in environmental water is much lower than the detection liminal value of the ICP-AES (0.01 mg/L), the samples were spiked with different Pb^{2+} concentrations, the analytical recoveries were in the acceptable range of 93-104% and 91-109% for the lake and tap water, respectively (Table S2), and the remain Pb^{2+} in the water samples after filtration was lower than the detection liminal value of ICP-AES, indicating that the DCA-PMDA NFM showed strong binding ability to Pb^{2+} .

Anti-interference ability and regeneration performance of DCA-PMDA . Theoretically, presence of Fe^{3+} , Cu^{2+} , Zn^{2+} , and Ca^{2+} would interfere the determination of Pb^{2+} to a greater or lesser extent due to competing retention onto PMDA. In this case, we tried to clear those aforementioned metal ions caused interference by adding IDA (1mM, 2 mL) to the samples Pb^{2+} solution (pH 6, 5 μM) and other metal ions solution (pH 6, 50 μM) prior to filtrate adsorption process. Fig. 6a shows the

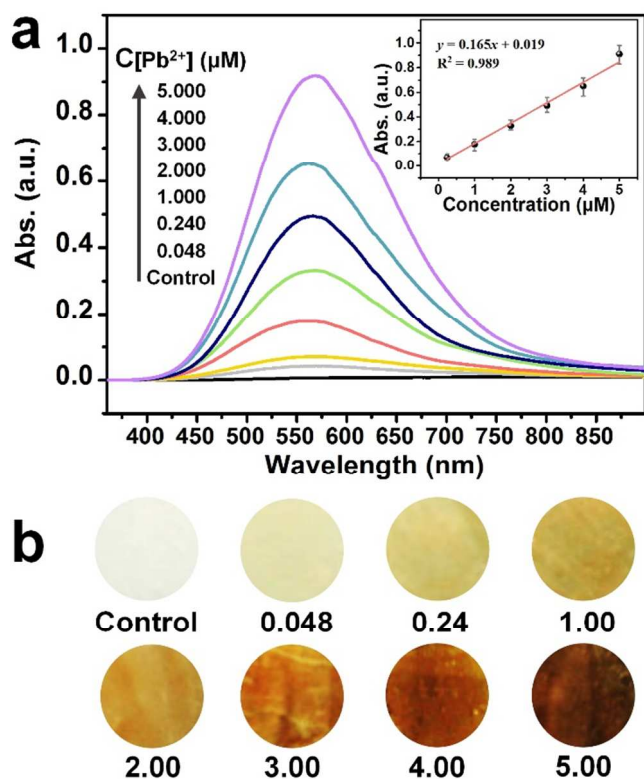


Fig. 6. (a) UV-Vis absorption spectra and (b) optical images of the strips after interacted with various concentration of Pb^{2+} .

changes (ΔA) in the absorption intensities at 560 nm before and after metal ions was filtrated ($\Delta A = A - A_0$, where A_0 and A were the absorption intensities of the strip in the absence and presence of metal ions, respectively). From the histogram illustrated in Fig. 6a, we can find that the ΔA induced by Pb^{2+} was 0.739, while for other metal ions, the ΔA aroused by them were negligible. The good anti-interference ability of strip could also be indicated by the optical images inset Fig. 6a, it is obvious that only the sample treated with Pb^{2+} solution showed a distinguishable color change from white to yellowish-brown, indicating the effective masking effort of IDA. And that also revealed presence of IDA itself did not interfere with the detection of Pb^{2+} .

Considering the economic plausibility of strip, it is very important that it should be able to reuse again for detection of Pb^{2+} . The ability of any sensor to detect the metal ions as well as to regenerate its active sites reduces the overall cost of the sensing process and makes the sensor more suitable, particularly for industrial applications. Desorption and the regeneration of adsorption sites could be achieved *via* treatment with an acidic solution (3 M HNO_3) for 1 min. The adsorption efficiency for Pb^{2+} for these ten successive cycles is presented in Fig. 6b. It was observed from the figure that the color changes of the strip after ten cycles of adsorption-desorption are keep constant. As shown in Fig. S6a, the HNO_3 treated sample remains wrinkled fiber surface and obviously adhesions among adjacent fibers, and the average fiber diameter has

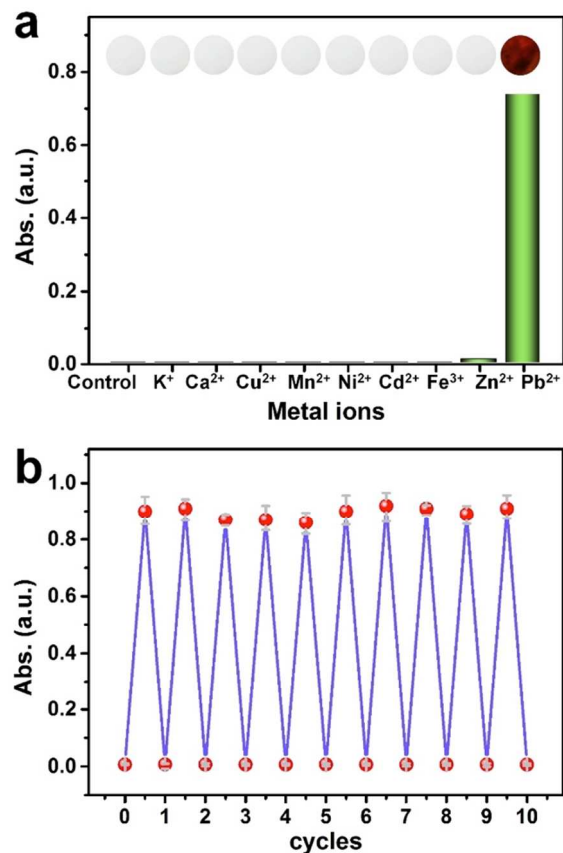


Fig. 7. (a) Colorimetric responses of strip after interacted with various metal ions for 30 min. (b) Performance of the strip during five cycles of regeneration for the adsorption-desorption of Pb^{2+} .

remained approximately constant after the treatment. Furthermore, in order to figure out the effect of HNO_3 treatment on chemical structure of strip, the FTIR study is performed. As shown in Fig. S6b, comparing with the spectrum of untreated strip, no significant changes were observed, especially the peak at 1723 cm^{-1} , representing the COOH groups in strip, suggesting that the HNO_3 treatment would not destroy the chemical structure and functionality.

Adsorption isotherm and maximum adsorption capacity.

In the final phase of our investigations, we ask how many Pb^{2+} was enriched on the $\text{DCA}_1\text{-PMDA}_3$ NFM during the sensing process in 30 min. To address this issue, the adsorption isotherm was applied here, which investigates the relationship between the Pb^{2+} concentrations in the solution and the amount of Pb^{2+} adsorbed on the solid phase when both phases are in the equilibrium position⁴⁸. To evaluate the adsorption isotherm, 50 mL of sample solutions containing various concentrations of Pb^{2+} (10, 20, 50, 100, and 200 μM) were adjusted pH of 6.0. At equilibrium, the filtrate solution was analyzed with ICP-AES to evaluate the remaining Pb^{2+} in each case and the data are displayed in Fig. 8a. The uptake efficiency of Pb^{2+} reached a plateau to obtain the maximum adsorption capacity was increased by increasing the initial concentrations and the

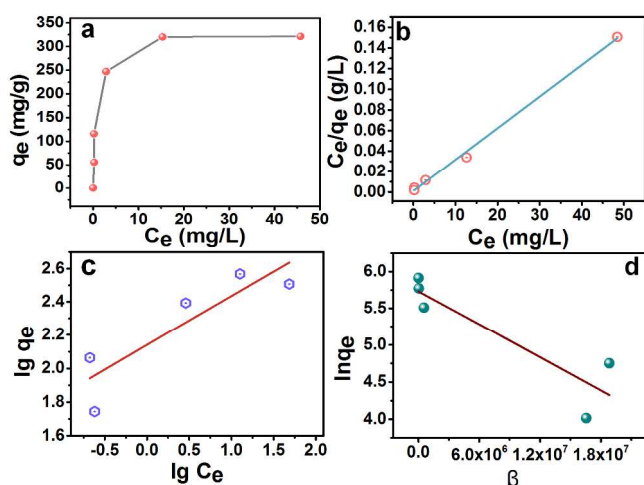


Fig. 7. (a) Adsorption isotherm for Pb^{2+} . The adsorption behavior analysis based on (b) Langmuir, (c) Freundlich and (d) Dubinin-Kaganer-Radushkevich modes.

decrease in the adsorbed amount is because that the active sites on the NFM surface were partially blocked by Pb^{2+} .

The interactive behavior between the $\text{DCA}_1\text{-PMDA}_3$ and Pb^{2+} at a particular temperature of 25°C as well as the feasibility of the process of adsorption are predicted using an adsorption isotherm. Here, three well-known models of Langmuir, Freundlich and Dubinin-Kaganer-Radushkevich (DKR) isotherms were used to evaluate the equilibrium data, and the applicability of the experimental data to an appropriate kinetic model was assessed by correlation coefficient (R^2). The values of different kinetics parameters calculated using different models are tabulated in Table S2. The linearized Langmuir isotherm model has been successfully applied to this adsorption operation as follows equation (2)⁴⁹: $C_e/q_e = 1/(K_L \times q_m) + 1/q_m \times C_e$ (linear form). Where, q_m is the maximum sorption capacity, K_L is the Langmuir sorption equilibrium constant. The q_m and K_L are the Langmuir constants which are related to the adsorption capacity and energy of adsorption, respectively, and can be calculated from the intercept and slope of the linear plot, with C_e/q_e versus C_e . From the fitting curve in Fig.8b, the R^2 is 0.9964 indicates good compliance with Langmuir model which describe a homogeneous adsorption surface, meaning that all the adsorption sites have equal adsorbate affinity. Another model, which we recruited, is Freundlich equation, it is an empirical equation employed to describe reversible adsorption and is not restricted to the formation of monolayer and predicts that the adsorbate concentrations on adsorbents would increase so long as there is an increase in the adsorbate concentration in solution⁵⁰. A linear form of the Freundlich expression can be obtained by taking logarithms of: $\ln q_e = \ln K_F + 1/n \times \ln C_e$ (linear form). Where, C_e is the equilibrium solution concentration (mg/L), K_F the Freundlich constant and $1/n$ the heterogeneity factor. Therefore, a plot of $\ln q_e$ versus $\ln C_e$ (Fig. 8c) enables the constant K_F and exponent $1/n$ to be determined. Based on these results, it can be deduced that the adsorption process is Langmuir monolayer adsorption rather than heterogeneous surface one. The reason might be related to the

electrostatic attraction between the $-\text{COOH}$ groups and Pb^{2+} , the effective ionic radii of Pb^{2+} in aqueous solution. These studies indicated that the adsorption of Pb^{2+} on the surface of $\text{DCA}_1\text{-PMDA}_3$ followed the monolayer process, which also confirmed the homogeneity of the PMDA on the surface of DCA. Moreover, based on the Langmuir isotherm model, it can be calculated that the q_m of Pb^{2+} is 326.80 mg/g. Furthermore, separation factor or equilibrium parameter (R_L) was used to predict the favorability of adsorption for L for adsorption process was represented by equation (4): $R_L = 1/(1 + K_L \times C_0)$. Where C_0 is the initial concentration of metal ion in solution (mg/L) and K_L is the adsorption intensity or Langmuir coefficient related to affinity of the binding sites⁵¹. After calculation, it was found that the R_L for $\text{DCA}_1\text{-PMDA}_3$ is between 0 and 1, which also confirms that the adsorption of Pb^{2+} was favorable.

In addition, DKR equation (5) was also used to analyze the experimental adsorption isotherms in Fig. 6d. The RKR model was the linear form⁵²: $\ln q_e = \ln q_{DR} - \beta \epsilon^2$. Where q_{DR} is the maximum adsorption capacity, β is the activity coefficient related to mean adsorption energy, and ϵ is the Polanyi potential, which is equal to $\epsilon = RT \ln(1 + 1/C_e)$. Where R is the gas constant (kJ/kmol·K), T is absolute temperature (K). However, the badness of fit of the experimental data could be told by R^2 . The DKR model showed better fit than Freundlich model, but worse than Langmuir isotherm model. The adsorption capacity (q_{DR} , 307.58 mg/g) obtained by utilizing the DKR model was found to be lower than the Langmuir adsorption capacity (326.80 mg/g). This difference in the adsorption capacities may be due to the different assumptions considered during the formulation of these isotherm models. **Comparative investigation.** The Pb^{2+} adsorption capacity and Pb^{2+} induced colorimetric response of various materials including CA NFM, DCA NFM, $\text{DCA}_1\text{-PMDA}_3$ NFM and filter paper-PMDA were studied. The adsorption isotherms for the

Table 1. Comparison of adsorption capacity of different NFM based adsorbents for the removal of Pb^{2+} .

NFM based adsorbent	q_m (mg/g)	refs
Polyacrylonitrile	223.21	53
(PAN)/polypyrrole/manganese dioxide	16	54
Dithizone embedded polystyrene	137.7	55
Thiol-modified cellulose composite	272.9	56
Chitosan/hydroxyapatite composite	23.75	34
$\text{SiO}_2@ \text{c-AIOOH}$ core/sheath fibers	260	57
PAN/polyethylene terephthalate	23.75	58
$\text{Fe}_2\text{O}_3\text{-Al}_2\text{O}_3$	214.8	59
PEO/Chitosan	41.4	60
Ethylenediamine/PAN/4-(2-pyridylazo)-1,3-benzenediol	217	61
Hydrazine-Modified PAN	326.8	This study

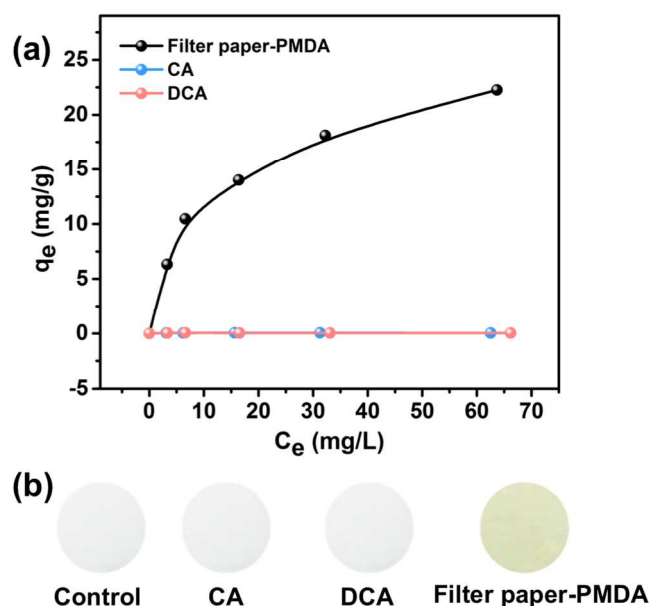


Fig. 8. (a) The adsorption isotherms for the adsorption of Pb²⁺ onto the CA, DCA, and filter paper-PMDA. (b) Their corresponding optical images after incubation with 5 μM Pb²⁺ and followed with Na₂S treatment.

adsorption of Pb²⁺ onto the CA, DCA and filter paper-PMDA are displayed in Fig. 8a, based on the Langmuir isotherm model, the calculated adsorption capacity of CA, DCA and filter paper-PMDA are 0.054, 0.067, and 25.73 mg/g, respectively, the extremely low capacity of CA and DCA NFM confirming the functionality of PMDA. Moreover, the adsorption capacity of filter paper-PMDA is 12.7 times smaller than that DCA-PMDA has, confirming that the tortuous porous structure and numerous interconnected microporous channels give DCA₁-PMDA₃ NFM a significant advantage as an adsorbent. The superiority of DCA₁-PMDA₃ could also be explained by the color changes show in Fig. 8b, it is obviously that only DCA₁-PMDA₃ NFM presents more obvious color change than other two NFM upon incubation with 5 μM Pb²⁺. The comparison results between DCA-PMDA and reported nanofibrous adsorbents are summarized in Table 1. It can be observed from the table that the adsorption capacity of the DCA-PMDA is superior to the adsorption capacities of the other NFM. Therefore, the high adsorption capacity of the DCA₁-PMDA₃ and its cost-effective and easy synthesis suggest its potential application for the treatment of industrially Pb²⁺ contaminated water.

Conclusion

To colorimetric detect and enrich low level toxic Pb²⁺ will lead to new frontiers in nanotechnology and materials science, and tunable and sensitive materials are essential. Therefore, the DCA-PMDA NFM fabricated in the present study exhibited interesting selective and reusable behavior that permits accurate, specific colorimetric detection of Pb²⁺ ions with low naked eye detection limit of 0.048 μM will show promising potential in Pb²⁺ contaminated water detection. The design of tunable DCA-

PMDA NFM was realized by modifying the PMDA ligand onto DCA NFM. Based on the strong interaction between PMDA and Pb²⁺, a color change from white to dark yellow-brown was observed at pH 6 and 30 min, respectively. Moreover, the enrichment of Pb²⁺ was underwent at the same time, and the maximum adsorption The adsorption isotherm data fitted well with the Langmuir isotherm models showed a maximum adsorption capacity of 326.80 mg/g. Therefore, the work has provided a generic and effective strategy to construct colorimetric materials for analyzing and enriching Pb²⁺ at a low concentration with a rapid-assessment process and open up ways for simply enriching various toxic ions without sophisticated instruments.

Acknowledges

This work is supported by the National Basic Research Program of China (973 Program, 2012CB525005), the National Natural Science Foundation of China (No. 51322304), and the “DHU Distinguished Young Professor Program”. The authors extend their appreciation to the Deanship of Scientific Research at King Saud University for funding the work through the international research group project no. IRG14-25.

Notes and references

^a Key Laboratory of Textile Science & Technology, Ministry of Education, College of Textiles, Donghua University, Shanghai 201620, China
^b College of Textiles, Zhongyuan University of Technology, Zhengzhou 450007, China

^c Petrochemical Research Chair, Department of Chemistry, College of Science, King Saud University, Riyadh 11451, Saudi Arabia

^d Department of Chemistry, Faculty of Science, Tanta University, Tanta 31527, Egypt

^e Nanomaterials Research Center, Modern Textile Institute, Donghua University, Shanghai 200051, China

† Electronic Supplementary Information (ESI) available: Photograph shows the experimental detailed of the setup for colorimetric detection and enrichment of Pb²⁺, FE-SEM images of (a) CA and (b) DCA NFM. Insets are the corresponding images at high magnification; EDX image of DCA₁-PMDA₃ after incubation with Pb²⁺ and followed by Na₂S color development reaction; FT-IR spectra of CA, DCA and DCA-PMDA NFM; reaction scheme for the modification of CA to DCA-PMDA, FE-SEM image (a) and FT-IR spectrum (b) of strip after treated with 3 M HNO₃ for 10 times. Inset is the corresponding image at high magnification; comparison of naked eye detect limit of different NFM based sensors for Pb²⁺; determination and removal of Pb²⁺ levels in real water samples; the rejection of DCA₁-PMDA₃ towards different concentration of Pb²⁺ in the feed solution; isotherm parameters for the adsorption of Pb²⁺ onto the DCA1-3 and supplementary references See DOI: 10.1039/b000000x/

1. S. M. Z. Hossain and J. D. Brennan, *Anal. Chem.*, 2011, **83**, 8772.
2. R. Prego and A. Cobelo-García, *Environ. Pollut.*, 2003, **121**, 425.
3. K. Jomova and M. Valko, *Toxicology*, 2011, **283**, 65.

4. K. Suresh Kumar, H.-U. Dahms, E.-J. Won, J.-S. Lee and K.-H. Shin, *Ecotoxicol. Environ. Saf.*, 2015, **113**, 329.
5. D.-L. Huang, G.-M. Zeng, C.-L. Feng, S. Hu, X.-Y. Jiang, L. Tang, F.-F. Su, Y. Zhang, W. Zeng and H.-L. Liu, *Environ. Sci. Technol.*, 2008, **42**, 4946.
6. S. Bouftini, J. Bahhou, B. Lelievre, J. M. C. de la Barca, A. Turcant, B. Diquet, S. Abourazzak, S. Chaouki, M. Hida, A. Khattabi, C. Nejari, A. Amarti and S. Achour, *Arch. Environ. Contam. Toxicol.*, 2015, **68**, 442.
7. B. Pourrut, M. Shahid, C. Dumat, P. Winterton and E. Pinelli, in *Reviews of Environmental Contamination and Toxicology Volume 213*, ed. D. M. Whitacre, Springer New York, 2011, pp. 113.
8. S. Tong, Y. E. von Schirmding and T. Prapamontol, *Bull. World Health Organ.*, 2000, **78**, 1068.
9. H. N. Kim, W. X. Ren, J. S. Kim and J. Yoon, *Chem. Soc. Rev.*, 2012, **41**, 3210.
10. N. S. La Colla, C. E. Domini, J. E. Marcovecchio and S. E. Botté, *J. Environ. Manage.*, 2015, **151**, 44.
11. G. Wu, H. Kang, X. Zhang, H. Shao, L. Chu and C. Ruan, *J. Hazard. Mater.*, 2010, **174**, 1.
12. A. Liu and R. D. Gonzalez, *Langmuir*, 2000, **16**, 3902.
13. Y.-H. Li, Z. Di, J. Ding, D. Wu, Z. Luan and Y. Zhu, *Water Res.*, 2005, **39**, 605.
14. W. S. Wan Ngah, L. C. Teong and M. A. K. M. Hanafiah, *Carbohydr. Polym.*, 2011, **83**, 1446.
15. S. C. B. Gopinath, T. Lakshmi Priya and K. Awazu, *Biosens. Bioelectron.* 2014, **51**, 115.
16. J. R. Askim, M. Mahmoudi and K. S. Suslick, *Chem. Soc. Rev.*, 2013, **42**, 8649.
17. Y. Guo, Z. Wang, W. Qu, H. Shao and X. Jiang, *Biosens. Bioelectron.*, 2011, **26**, 4064.
18. F. Zapata, A. Caballero, A. Espinosa, A. Tarraga and P. Molina, *Org. Lett.*, 2007, **10**, 41.
19. M. R. Awual and M. M. Hasan, *Micropor. Mesopor. Mat.*, 2014, **196**, 261.
20. M. R. Awual and M. M. Hasan, *Sensor. Actuat. B-Chem.*, 2014, **202**, 395.
21. I. Nischang, I. Teasdale and O. Brüggemann, *Anal. Bioanal. Chem.*, 2011, **400**, 2289.
22. X. Wang, B. Ding, G. Sun, M. Wang and J. Yu, *Prog. Mater. Sci.*, 2013, **58**, 1173.
23. M. M. Khin, A. S. Nair, V. J. Babu, R. Murugan and S. Ramakrishna, *Energy Environ. Sci.*, 2012, **5**, 8075.
24. S. Su, W. Wu, J. Gao, J. Lu and C. Fan, *J. Mater. Chem.*, 2012, **22**, 18101.
25. Y. Li, Y. Si, X. Wang, B. Ding, G. Sun, G. Zheng, W. Luo and J. Yu, *Biosens. Bioelectron.*, 2013, **48**, 244.
26. Y. Li, L. Wang, X. Yin, B. Ding, G. Sun, T. Ke, J. Chen and J. Yu, *J. Mater. Chem. A*, 2014, **2**, 18304.
27. Y. Li, B. Ding, G. Sun, T. Ke, J. Chen, S. S. Al-Deyab and J. Yu, *Sensor. Actuat. B-Chem.*, 2014, **204**, 673.
28. B. Ding, M. Wang, X. Wang, J. Yu and G. Sun, *Materials Today*, 2010, **13**, 16.
29. T. Vasudevan, A. K. Pandey, S. Das and P. K. Pujari, *Chem. Eng. J.*, 2014, **236**, 9.
30. H.-W. Liang, X. Cao, W.-J. Zhang, H.-T. Lin, F. Zhou, L.-F. Chen and S.-H. Yu, *Adv. Funct. Mater.*, 2011, **21**, 3851.
31. P. Kampalanonwat and P. Supaphol, *ACS Appl. Mater. Inter.*, 2010, **2**, 3619.
32. Y.-X. Yu, *ACS Appl. Mater. Inter.*, 2014, **6**, 16267.
33. J.-X. Yu, R.-A. Chi, X.-Z. Su, Z.-Y. He, Y.-F. Qi and Y.-F. Zhang, *J. Hazard. Mater.*, 2010, **177**, 222.
34. Y. Huang, Y.-E. Miao and T. Liu, *J. Appl. Polym. Sci.*, 2014, **131**, 39877/1.
35. Y. Xing, X.-M. Sun and B.-H. Li, *Environ. Eng. Sci.*, 2008, **26**, 551.
36. S. K. Papageorgiou, E. P. Kouvelos, E. P. Favvas, A. A. Sapalidis, G. E. Romanos and F. K. Katsaros, *Cat. Rev.*, 2010, **345**, 469.
37. M. I. Boyanov, J. Kmetko, T. Shibata, A. Datta, P. Dutta and B. A. Bunker, *J. Phys. Chem. B*, 2003, **107**, 9780.
38. Z. Ma, M. Kotaki and S. Ramakrishna, *J. Membr. Sci.*, 2005, **265**, 115.
39. L. Zhang, T. J. Menkhaus and H. Fong, *J. Membr. Sci.*, 2008, **319**, 176.
40. X. Wang, Y. Li, X. Li, J. Yu, S. S. Al-Deyab and B. Ding, *Sensor. Actuat. B-Chem.*, 2014, **203**, 333.
41. S. Deng and Y. P. Ting, *Langmuir*, 2005, **21**, 5940.
42. Y. Si, J. Yu, X. Tang, J. Ge and B. Ding, *Nat. Commun.*, 2014, **5**, 5802.
43. J. Huang and R. B. Kaner, *J. Am. Chem. Soc.*, 2004, **126**, 851-855.
44. Y. J. Ryu, H. Y. Kim, K. H. Lee, H. C. Park and D. R. Lee, *Eur. Polym. J.*, 2003, **39**, 1883.
45. Q. Dong, J. Liu, L. Song and G. Shao, *J. Hazard. Mater.*, 2011, **186**, 1335.
46. H. Mittal, A. Maity and S. Sinha Ray, *J. Phys. Chem. B*, 2015, **119**, 2026.
47. A. Esmaeili and A. A. Beni, *J. Hazard. Mater.*, 2014, **280**, 788.
48. S. Ghorai, A. Sarkar, M. Raoufi, A. B. Panda, H. Schönherr and S. Pal, *ACS Appl. Mater. Inter.*, 2014, **6**, 4766.
49. I. Langmuir, *J. Am. Chem. Soc.*, 1916, **38**, 2221.
50. G. Annadurai, R.-S. Juang and D.-J. Lee, *J. Hazard. Mater.*, 2002, **92**, 263.
51. G. Moussavi and R. Khosravi, *J. Hazard. Mater.*, 2010, **183**, 724.
52. P. Chutia, S. Kato, T. Kojima and S. Satokawa, *J. Hazard. Mater.*, 2009, **162**, 440.
53. C. Luo, J. Wang, P. Jia, Y. Liu, J. An, B. Cao and K. Pan, *Chem. Eng. J.*, 2015, **262**, 775.
54. J. Deng, X. Kang, L. Chen, Y. Wang, Z. Gu and Z. Lu, *J. Hazard. Mater.*, 2011, **196**, 187.
55. R. Yang, K. B. Aubrecht, H. Ma, R. Wang, R. B. Grubbs, B. S. Hsiao and B. Chu, *Polymer*, 2014, **55**, 1167.
56. M. Aliabadi, M. Irani, J. Ismaeili and S. Najafzadeh, *J. Taiwan Inst. Chem. E.*, 2014, **45**, 518.
57. R. Wang, S. Guan, A. Sato, X. Wang, Z. Wang, R. Yang, B. S. Hsiao and B. Chu, *J. Membr. Sci.*, 2013, **446**, 376.
58. A. Mahapatra, B. G. Mishra and G. Hota, *J. Hazard. Mater.*, 2013, **258-259**, 116.
59. M. Aliabadi, M. Irani, J. Ismaeili, H. Piri and M. J. Parnian, *Chem. Eng. J.*, 2013, **220**, 237.
60. G. Li, L. Zhang, Z. Li and W. Zhang, *J. Hazard. Mater.*, 2010, **177**, 983.
61. K. Saeed, S.-Y. Park and T.-J. Oh, *J. Appl. Polym. Sci.*, 2011, **121**, 869.